Organic & Biomolecular Chemistry

Accepted Manuscript

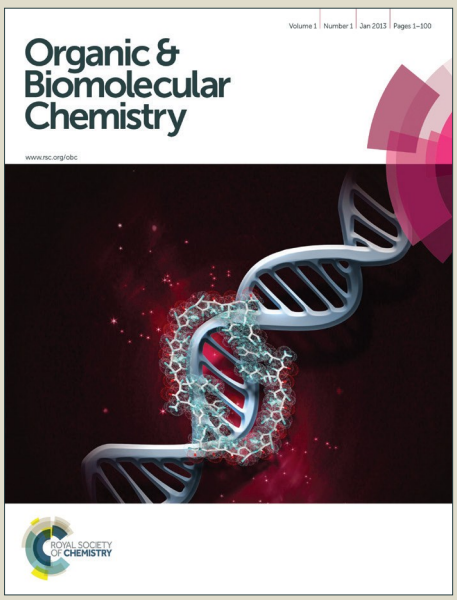

ROYAL SOCIETY OF CHEMISTRY

www.rsc.org/obc

Journal Name

RSCPublishing

ARTICLE

In Vitro Selectivity of an Acyclic Cucurbit[*n*]uril Molecular Container towards Neuromuscular Blocking Agents Relative to Commonly Used Drugs

Cite this: DOI: 10.1039/x0xx00000x

Received 00th January 2012,
Accepted 00th January 2012

DOI: 10.1039/x0xx00000x

www.rsc.org/

Shweta Ganapati,[†] Peter Y. Zavalij,[†] Matthias Eikermann*[,‡] Lyle Isaacs*[,†]

An acyclic cucurbit[*n*]uril (CB[*n*]) based molecular container (**2**, a.k.a. Calabadion 2) binds to both amino-steroidal and benzylisoquinolinium type neuromuscular blocking agents (NMBAs) *in vitro*, and reverses the effect of these drugs *in vivo* displaying faster recovery times than placebo and the γ-cyclodextrin (CD) based and clinically used reversal agent Sugammadex. In this study we have assessed the potential for other drugs commonly used during and after surgery (e.g. antibiotics, antihistamines, and antiarrhythmics) to interfere with the ability of **2** to bind NMBAs rocuronium and cisatracurium *in vitro*. We measured the binding affinities (K_a, M^{-1}) of twenty seven commonly used drugs towards **2** and simulated the equilibrium between **2**, NMBA, and drug based on their standard clinical dosages to calculate the equilibrium concentration of **2**•NMBA in the presence of the various drugs. We found that none of the 27 drugs studied possess the combination of a high enough binding affinity with **2** and a high enough standard dosage to be able to promote the competitive dissociation (a.k.a. displacement interactions) of the **2**•NMBA complex with the formation of the **2**•drug complex. Finally, we used the simulations to explore how the potential for displacement interactions is affected by a number of factors including the K_a of the **2**•NMBA complex, the K_a of the AChR•NMBA complex, the K_a of the **2**•drug complex, and the dosage of the drug.

Introduction

Annually, more than 400 million patients receive curare-type neuromuscular blocking agents (NMBAs) during surgical procedures in operating rooms, intensive care units, and emergency medicine departments.[1] NMBAs such as rocuronium and cisatracurium are often used as an essential adjunct to general anesthesia to block neuromuscular transmission (muscle relaxation) dose-dependently which facilitates endotracheal intubation, optimizes surgical conditions, and prevents potentially harmful movements during surgery. To speed up the recovery of the muscle function of the patient and to prevent residual neuromuscular block, it is often necessary to reverse the biological effect of NMBAs at the end of the surgery.[2] A major advance in the clinical practice of anesthesia was made by the introduction of a γ-cyclodextrin-derived molecular container known as Sugammadex (**1**, marketed as Bridion™ by Merck with sales of more than $340 million in 2014; Figure 1), which binds rocuronium with high affinity ($K_a = 1.05 \times 10^7$ M^{-1}) in water and reverses the effects of rocuronium *in vivo*.[3] Compound **1** reverses neuromuscular block by sequestering rocuronium in the bloodstream, thereby depleting its concentration at the neuromuscular junction.[4] The **1**•rocuronium complex is subsequently excreted in the urine. Compound **1** has had a major impact on the clinical practice of anesthesia in Europe but use in the United States has been delayed by the US FDA because of hypersensitivity events.[5] As a result, there is a real need to develop alternative classes of molecular containers that function as reversal agents for the full range of clinically important NMBAs.

We, and others, have been studying the synthesis and supramolecular chemistry of a new family of molecular containers known as cucurbit[*n*]urils (CB[*n*], Figure 1), which comprise n glycoluril rings linked by 2*n* methylene bridges.[6,7] The defining structural features of CB[*n*] molecular containers are a hydrophobic cavity guarded by two symmetry-equivalent electrostatically negative ureidyl C=O portals.[6,8] The carbonyl portals facilitate ion-dipole and hydrogen bonding interactions with the ammonium groups of guests whereas the inclusion of the hydrophobic residues in the CB[*n*] cavity delivers a hydrophobic driving force due to expulsion of high energy water molecules present in the cavity of the free container.[9,10,11] Accordingly, CB[*n*] compounds display unusually high affinity (K_a commonly reaches 10^9 M^{-1}) toward alkane (di)ammonium

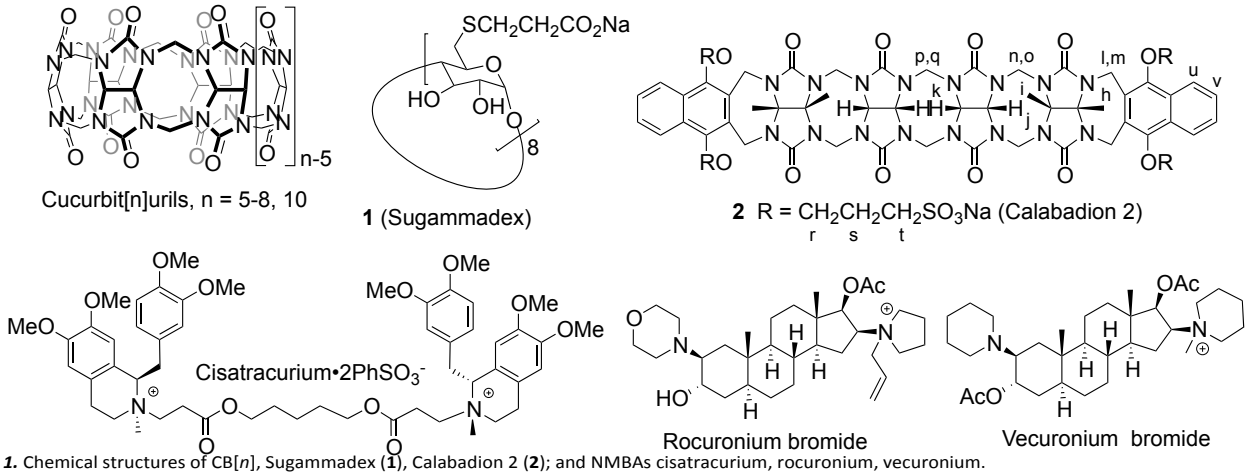

Figure 1. Chemical structures of CB[*n*], Sugammadex (**1**), Calabadion 2 (**2**); and NMBAs cisatracurium, rocuronium, vecuronium.

ions in water.[9,10,12,13] As a result of the high affinity and high selectivity displayed by CB[*n*] compounds toward their guests, they have been used in a variety of applications including stimuli-responsive molecular machines, sensing ensembles, biomimetic processes, supramolecular polymers, (targeted) drug delivery, and drug reversal.[14] Given the high K_a values typically observed for CB[*n*]•guest complexes, we realized that CB[*n*]-type receptors represent a potential alternative to the γ-cyclodextrin derivative Sugammadex (**1**) for the reversal of neuromuscular block. Among the known CB[*n*], only CB[8] and CB[10] are large enough to encapsulate the steroidal nucleus of NMBAs like rocuronium, but unfortunately the water solubility of these containers is poor (<100 μm) which severely limits their potential to function as *in vivo* reversal agents for NMBAs. Conversely, water-soluble CB[7] is neither voluminous enough to encapsulate the steroidal ring system nor is its C=O···O=C distance of ~ 6.1 Å appropriate to electrostatically complement the N···N separation (~ 11.0 Å) of the steroidal NMBAs rocuronium and vecuronium. In fact, Macartney has shown that CB[7] binds to the ammonium ends of the steroidal NMBAs rather than the steroidal ring system.[15]

Recently, we have introduced acyclic CB[*n*]-type receptors that feature a central glycoluril tetramer, two aromatic walls and four sulfonate solubilizing groups.[16,17,18] Compound **2** is a prototypical member of this class of CB[*n*]-type receptors. We have found that acyclic CB[*n*] compounds function as potent receptors for a wide variety of compounds in water including not only standard CB[*n*] guests (e.g. alkane diammonium ions) but also for carbon nanotubes, nitrosamines, and insoluble drugs.[18,19] In 2012 we reported that acyclic CB[*n*]-type receptor **2** binds steroidal NMBAs 100-fold stronger and the benzylisoquinoline type NMBA cisatracurium 1000-fold stronger than **1** in water.[17] *In vivo* experiments in rats showed that **2** reverses deep neuromuscular blockade induced by steroidal NMBAs rocuronium and vecuronium in a dose dependent manner and restores the train-of-four ratio to 0.9 faster than placebo and **1**.[17,20,21] The same trend is observed for recovery of spontaneous breathing, which is also rapid with **2** as compared to experiments using placebo or **1**.[17] Unlike Sugammadex (**1**), Calabadion 2 (**2**) displays a high *in vitro* binding affinity towards cisatracurium and also causes the *in vivo* reversal of the benzylisoquinolinium NMBA cisatracurium.[20,21] These previously published *in vivo* and *in vitro* results together indicate the potential of **2** to act as a broad spectrum reversal agent of NMBAs. However, there is the possibility that a patient who has been or is being treated with NMBAs during surgery may have previously taken other drugs and/or need to be treated with other drugs post-surgically. For example, many surgical patients are treated with a variety of other drugs including antibiotics, antihistamines, and antiarrhythmics.[22] Accordingly, for the further development of **2** it is important to assess whether the binding of **2** toward rocuronium, vecuronium, or cisatracurium can be compromised by the presence of other drugs. In this paper, we determine the binding constant of **2** toward 27 drugs that are commonly used during and after surgery and assess the potential for these 27 drugs to induce displacement of rocuronium, vecuronium, or cisatracurium from the cavity of **2** by the use of numerical simulations of the multicomponent system using Gepasi™.[23] These drugs were selected to include a variety of drug classes such as antibiotics, antiarrythmics, analagesics, etc. which are typically present on standard anesthesia trays at hospitals. Cationic drugs were selected specifically as they are expected to have higher affinity towards our anionic acyclic CB[n]-type container **2**, and therefore pose the highest potential for displacing NMBAs from the **2**•NMBA complexes.

Results and discussion

This results and discussion section is organized as follows. First, we describe the investigation of the binding properties of **2** toward drugs **3**-**29** (Figure 2) by ^{1}H NMR spectroscopy. Next, we measure the binding affinities (K_a, M^{-1}) of **2** toward each drug using either direct ^{1}H NMR titration or UV/Vis binding assays (direct or competition). Finally, we use the experimentally determined values of K_a as known inputs to

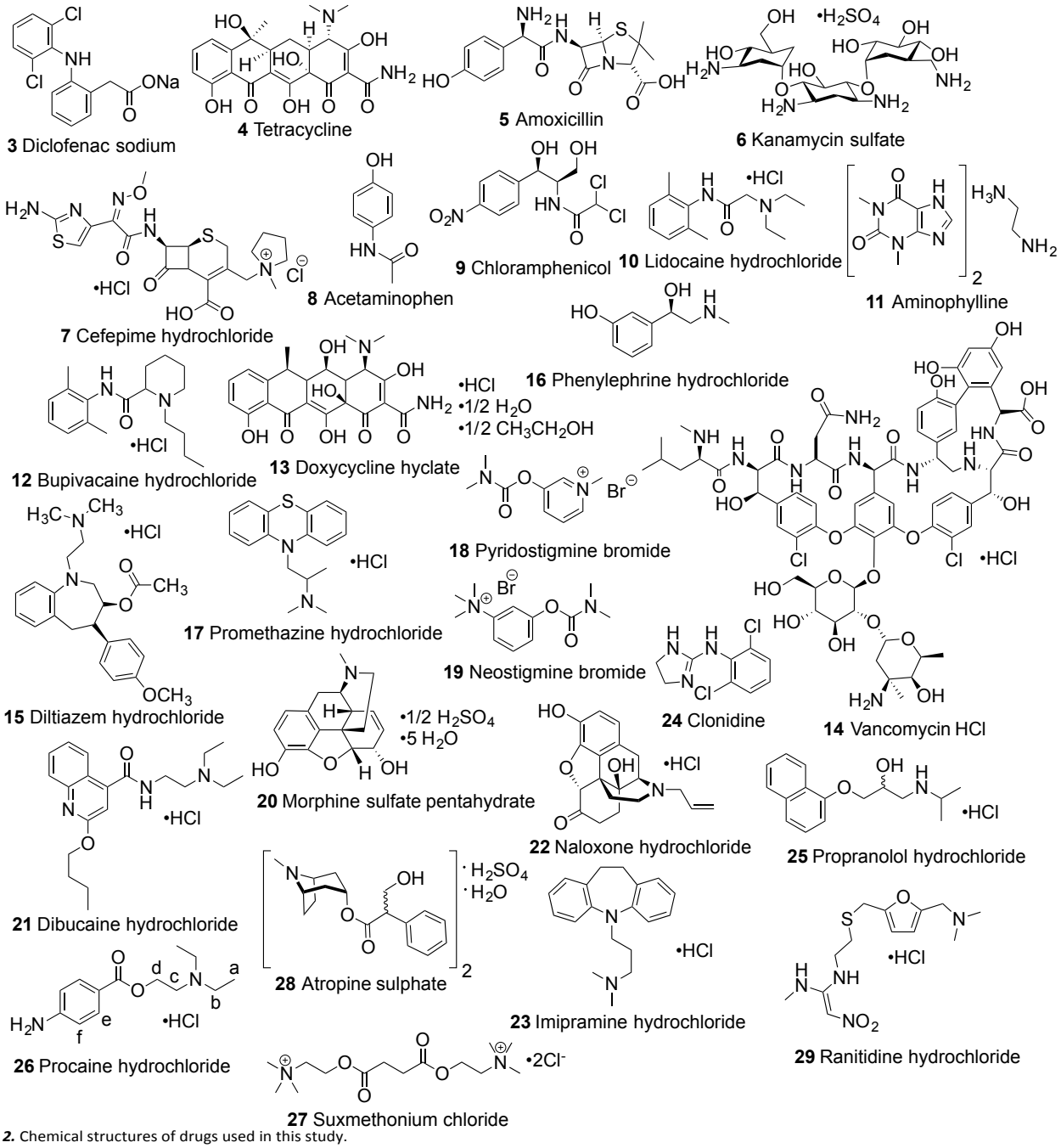

Figure 2. Chemical structures of drugs used in this study.

explore by simulations (Gepasi™) the behavior of the multicomponent system comprising **2**, rocuronium or vecuronium or cisatracurium, acetylcholine receptor (AChR), and drug using estimated or known values of clinical drug concentration ranges and AChR binding constants. The results of these simulations are presented in the form of three dimensional plots that connect the binding affinity of the **2**•drug complex and the dosage of drug with the equilibrium concentration of the AChR•NMBA complex.

Binding properties of 2 towards drugs 3 – 29 investigated by ^{1}H NMR. Initially, we investigated the ability of container **2** to bind drugs **3** – **29** by ^{1}H NMR spectroscopy. For complexes between **2** and drugs **3** – **29** we commonly observed upfield shifting of guest resonances which indicates that these protons on the guest (drug) are located in the cavity of **2**. All of the **2**•drug complexes display intermediate to fast kinetics of exchange on the ^{1}H NMR timescale. These preliminary ^{1}H NMR observations suggested that complexes between container **2** and drugs **3**–**29** would be of moderate stability in water. In contrast, complexes between **2** and NMBAs cisatracurium, rocuronium and vecuronium exhibit slow exchange on the chemical shift timescale. To facilitate further discussion of the

NMR results we present the ^{1}H NMR spectra recorded for **26** (procaine), **2**, the **2•26** complex, and a mixture of **2•26** with excess **26** present (Figure 3). These ^{1}H NMR spectra display a number of interesting features, which provide insight the nature of the **2•26** complex. For example, the aromatic peaks H_e, and H_f of **26** shift considerably upfield (> 1 ppm) upon binding to one equivalent of **2** (Figure 3c). This dramatic upfield shift reflects the anisotropic shielding environment provided by the two aromatic naphthalene sidewalls of **2**. Given the aromatic nature of drug **26**, we surmise that π–π interactions are formed within the **2•26** complex. In the spectrum containing two equivalents of **26** to one equivalent of **2** (Figure 3d) H_e and H_f shift back downfield (relative to Figure 3c) to a position that is the average of the completely bound and completely free form of **26**. This indicates a fast kinetics of exchange between free guest **26** and the **2•26** complex relative to the ^{1}H NMR chemical shift time scale. In contrast, the aromatic protons H_u and H_v of host **2** undergo a downfield shift (H_u, 7.72 ppm; H_v, 7.17 ppm) upon formation of the **2•26** complex. The observed downfield shift is due to the disruption of edge-to-face π–π interactions between the tips of free host **2** which are disrupted upon formation of the **2•26** complex. Addition of a second equivalent of **26** results in little additional shifting and sharpening of the resonances for H_u and H_v because the **2•26** complex is largely formed at both stoichiometries. Interestingly, the resonances for H_a, H_b, and H_c of 2-diethylaminoethyl sidechain also show significant upfield shifts upon binding to **2** which is probably reflects partial inclusion of the sidechain in the shielding region defined by the glycoluril tetramer backbone and the aromatic naphthalene sidewalls. Analogous phenomena were seen in the ^{1}H NMR spectra recorded for the remaining **2**•drug complexes in accord with the previously established preferences of CB[n]-type receptors to bind the hydrophobic portions of guests within the hydrophobic cavity whereas the cationic ammonium groups groups reside at the ureidyl carbonyl portals and benefit from ion-dipole interactions.[9]

Stoichiometry of the Complexes Between 2 and Drugs 3 – 29. It is well known that CB[n]-type receptors generally form host•guest complexes with 1:1 stoichiometry. In order to confirm the 1:1 stoichiometry of the complexes between **2** and drugs **3** – **29** we created Job plots.[24] In Job plots, a series of samples containing host and guest at a constant total concentration ([host] + [guest] = constant) are prepared and are investigated by an appropriate spectroscopic technique. A plot of the change in spectroscopic signal versus mole fraction displays a maximum at the mole fraction that corresponds to the stoichiometry of the host•guest complex. Figure 4 shows the Job plot constructed using **2** and **26** at a total concentration of 1 mM. The Job plot displays a maximum at a mole fraction of 0.5 which confirms the 1:1 stoichiometry of the **2•26** complex. Job plots were constructed for several additional drugs and are given in the Supporting Information.

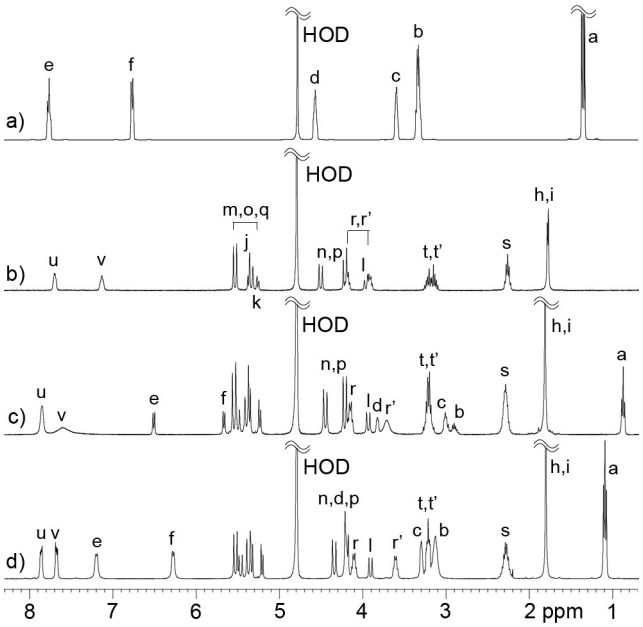

Figure 3. ^{1}H NMR spectra recorded (400 MHz, RT, 20 mM NaH_2PO_4 buffered D_2O, pH = 7.4) for a) **26**, b) **2**, c) an equimolar mixture of **2** and **26** (12.5 mM), and d) a 1:2 mixture of **2** (12.5 mM) and **26** (25 mM).

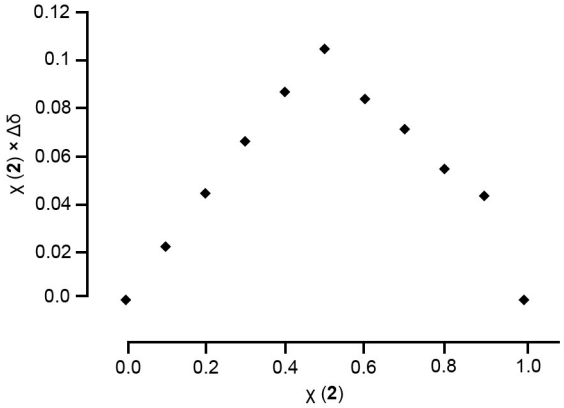

Figure 4. Job plot constructed for mixtures of **2** and **26** ([**2**] + [**26**] = 1 mM) by monitoring the change in ^{1}H NMR (400 MHz, RT, 20 mM NaH_2PO_4 buffered D_2O, pH = 7.4) chemical shift of H_u (7.72 ppm) of **2**.

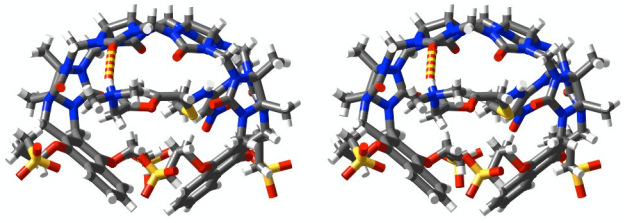

Figure 5. Cross-eyed stereoscopic represention of the geometry of one molecule of **2•29** from the x-ray crystal structure. Color code: C, grey; H, white; N, blue; O, red; S, yellow; hydrogen bond, red–yellow striped.

X-ray Crystal Structure of the 2•29 Complex. We were fortunate to obtain single crystals of the **2•29** complex by slow evaporation of an aqueous solution of the complex and to solve its x-ray crystal structure. Figure 5 shows a cross-eyed stereoview of one molecule of **2•29** in the crystal which

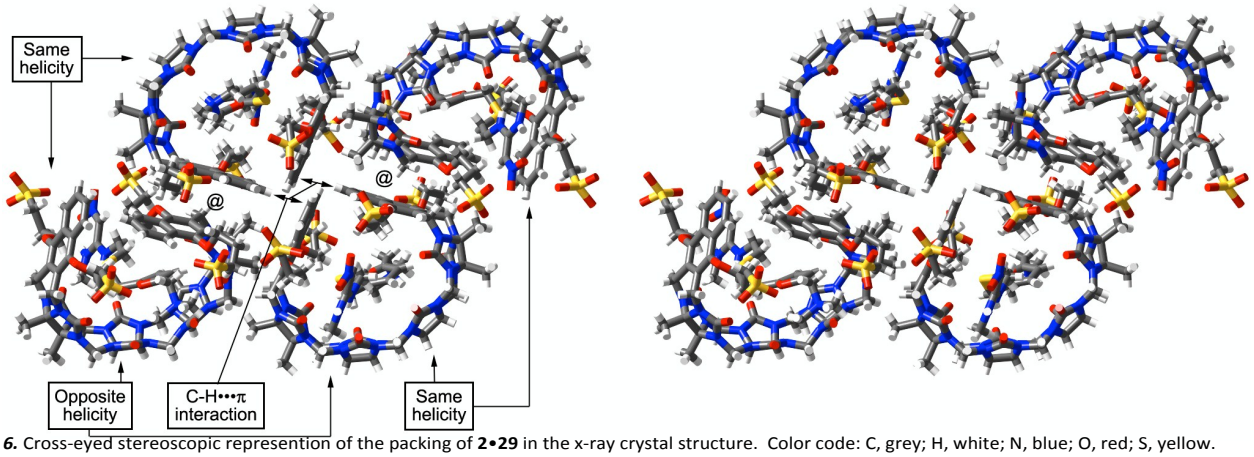

Figure 6. Cross-eyed stereoscopic represention of the packing of **2•29** in the x-ray crystal structure. Color code: C, grey; H, white; N, blue; O, red; S, yellow.

displays a number of interesting features. As described previously, the glycoluril tetramer backbone of **2** imparts an overall C-shape to the receptor whereas the terminal napthalene sidewalls help to define a hydrophobic box-like cavity. Interestingly, host **2** within the **2•29** complex adopts a helical (chiral) conformation where the two naphthalene sidewalls are splayed out-of-plane with respect to the glycoluril tetramer backbone; both senses of handedness are observed in the crystal in a 1:1 ratio. Furthermore, the ammonium ion unit of guest **29** engages in an N-H•••O=C hydrogen bond (N•••O distance = 2.803 Å; N-H•••O angle = 160.9˚) with the carbonyl portal. The furan ring is enclosed within the cavity of **2** but does not engage in π–π stacking interactions with naphthalene sidewalls. In addition, one of the amidine N-H groups at the opposite carbonyl portal appears to engage in a weak hydrogen bond (N•••O distance = 3.231 Å; N-H•••O angle = 147.2˚) Finally, Figure 5 shows that the naphthalene sidewalls of **2** in the **2•29** complex do not undergo edge-to-face π–π interactions which is in accord with the downfield shift observed for H_u and H_v upon complex formation.[17,25] The three dimensional packing of the individual molecules of **2•29** complex in the crystal is also intriguing (Figure 6). As shown in Figure 6, two molecules of the **2•29** complex of the same helicity pack next to one another by interactions between the convex faces of the aromatic sidewalls (marked with @ symbol). Additional homochiral pairs of the **2•29** complex extend along the z-axis with alternating sense of helicity. Quite interestingly, adjacent pairs of the **2•29** complex are held together by reciprocal pairs of close CH•••π interactions (CH•••π distance = 2.798, 2.868 Å; CH•••π angle = 161.7˚, 149.1˚) between molecules of complex **2•29** of opposite helicity.

Measurement of Binding affinities between 2 and drugs 3-29. After having established the inclusion binding of drugs **3** – **29** inside container **2** by ^{1}H NMR spectroscopy, we decided to measure the binding affinity (K_a, M^{-1}) for the **2•3** – **2•29** complexes. For this purpose, we employed three different strategies: 1) direct UV/Vis titrations (for UV/Vis active drug **4**), 2) direct ^{1}H NMR titrations (for drugs **3**, **5**-**7**, **9**, **11**, and **13** with K_a < 5000 M^{-1}), and 3) UV/Vis competition titrations (for UV/Vis inactive drugs with K_a > 5000 M^{-1}). The detailed procedures and models used to analyze the data using Scientist™ are given in the Supporting Information. For example, Figure 7a shows the ^{1}H NMR spectra recorded during the titration of a fixed concentration of **2** (0.976 mM) with **6** (0 – 6.57 mM). As described above, upon formation of the **2**•guest complexes, we generally observe a downfield shift of H_u and H_v because the tips of the naphthalene sidewalls are no longer engaged in edge-to-face π–π interactions. Figure 7b shows a plot of chemical shift of H_v versus [**6**] which was fitted to a standard 1:1 binding model using Scientist™ (Supporting Information) which allowed us to determine $K_a = (3.0 \pm 0.6) \times 10^3$ M^{-1} for the **2•6** complex. Similar ^{1}H NMR titrations were performed for guests **3**, **5** - **7**, **9**, **11**, and **13** (Supporting Information) and the results are presented in Table 1.

Next, to determine the K_a values for the stronger **2**•guest complexes we performed competition experiments monitored by UV/Vis spectroscopy.[26] For this purpose, we employed Rhodamine 6G which undergoes significant changes in its UV/Vis spectrum upon formation of the **2**•Rhodamine 6G complex ($K_a = 2.3 \pm 0.2 \times 10^6$ M^{-1}).[17] Addition of competitive guests displace indicator Rhodamine 6G from the **2**•Rhodamine 6G complex and reverse the observed UV/Vis changes. Figure 8 shows the absorbance data obtained from the competitive UV/Vis titration of **2**•Rhodamine 6G with **28** (0 – 1.21 mM). We fit a plot of absorbance versus [**28**] to the standard competitive binding model (Supporting Information)[17,19] to determine the K_a for the **2•28** complex ($K_a = (3.3 \pm 0.5) \times 10^6$ M^{-1}) using the known K_a of **2**•rhodamine 6G ($(2.3 \pm 0.2) \times 10^6$ M^{-1})[17] as input. Analogous UV/Vis competition experiments were performed which allowed us to measure the remaining K_a values given in Table 1. For purposes of comparison, the K_a values for Sugammadex (**1**) toward drugs **3** – **29** as reported by Zwiers are also given in Table 1.[22]

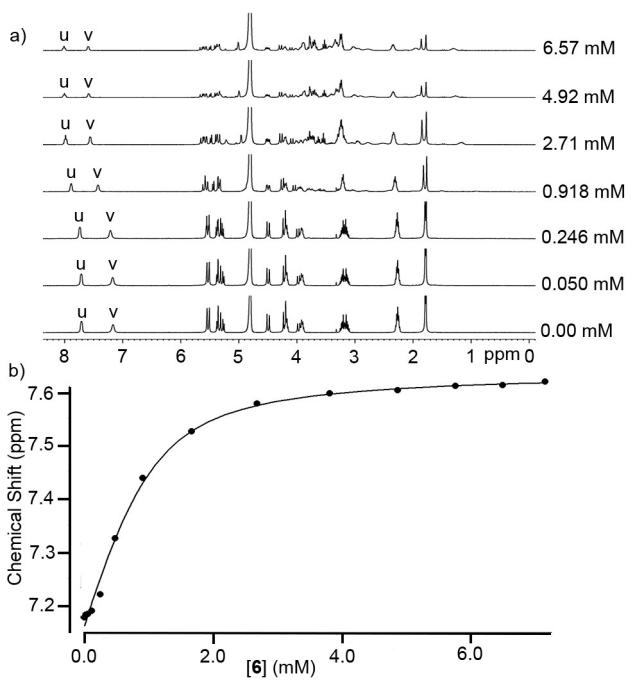

Figure 7. a) ^{1}H NMR (400 MHz) stack plot of the titration of **2** (0.976 mM) with guest **6** (0 – 6.57 mM) in 20 mM NaH_2PO_4 buffered D_2O (pH = 7.4); b) plot of the chemical shift of H_v as a function of guest concentration. The solid line represents the best non-linear fit of the data to a 1:1 model ($K_a = (3.0 \pm 0.6) \times 10^3$ M^{-1}).

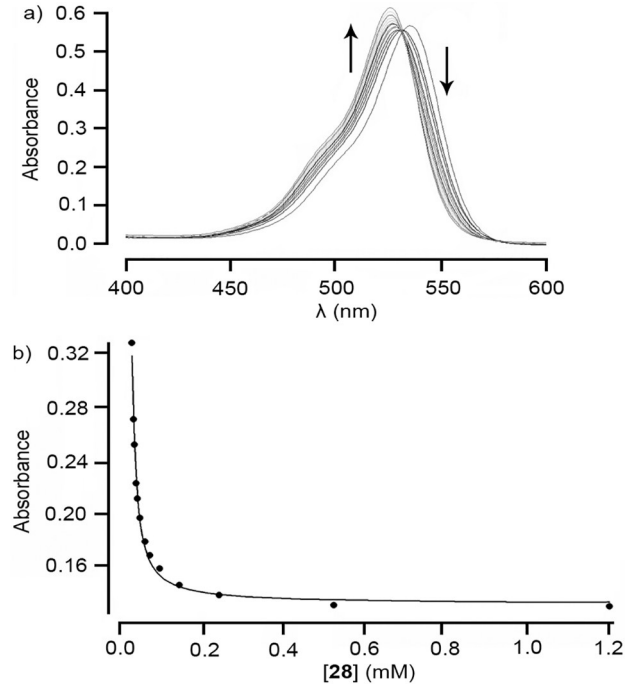

Figure 8. a) UV/Vis spectra recorded during the titration of a mixture of **2** (9.92 μM) and dye rhodamine 6G (10.0 μM) with guest **28** (0 – 1.21 mM) in 20 mM NaH_2PO_4 buffer (pH = 7.4), b) plot of absorbance at 550 nm as a function of the concentration of **28**. The solid line represents the best non-linear fit of the data to a competitive binding model ($K_a = (3.3 \pm 0.5) \times 10^6$ M^{-1}).

Commentary on the Tabulated K_a Values. An examination of the binding constants given in Table 1 reveals that the K_a values for this set of 27 drugs ranges from a low of 2.0 x 10^3 M^{-1} for diclofenac **3** to a high of 4.5 x 10^6 M^{-1} for ranitidine **29**; 13 out of 27 drugs have $K_a > 10^5$ M^{-1} whereas 14 out of 27 have $K_a < 10^5$ M^{-1}. Some of the trends can be readily understood given the well-known binding preferences of CB[n] and acyclic CB[n]-type receptors for hydrophobic and (di)cationic guests.[9] For example, among the weaker binders ($K_a < 10^5$ M^{-1}) we find neutral or anionic compounds like diclofenac (**3**), acetaminophen (**8**), chloramphenicol (**9**), and aminophylline (**11**) as well as highly hydrophilic and hydroxylated compounds like tetracycline (**4**), kanamycin (**6**), doxycycline (**13**), and vancomycin (**14**). Other weak binders include the zwitterionic compounds amoxicillin (**5**) and cefepime (**7**). Conversely, among the stronger binders ($K_a > 10^5$ M^{-1}) we find compounds that better satisfy the binding preferences of **2**. For example, the two linear dications procaine (**26**) and suxmethonium chloride (**27**) are among the strongest binding drugs. In accord with the preference of CB[n]-type receptors for hydrophobic bicyclic and polycyclic cations,[6,9,12,27] compounds like morphine (**20**), naloxone (**22**), atropine (**28**) are among the better binders for **2**. Recently, we reported that **2** is an outstanding solubilizing agent for insoluble drugs that are aromatic cations due to the formation of π–π interactions between the insoluble drug and the naphthalene walls of **2** which define a hydrophobic box.[25] The observed stronger binding between **2** and aromatic ammonium ions dibucaine (**21**), propranolol (**25**), and imipramine (**23**) are consistent with the previously delineated binding preferences of **2**.

Assessment of the Potential for Displacement Interactions. We undertook the measurement of the binding constants for the complexes between **2** and drugs **3** – **29** with the goal of assessing the potential for these drugs to interfere with the *in vivo* use of **2** as a reversal agent for neuromuscular block induced by rocuronium, vecuronium, or cisatracurium. Given the high level of complexity of the *in vivo* system (e.g. metabolism, excretion, biodistribution, other binding partners) we created a minimalist model that is amenable to appropriate simulations. Figure 9 shows the three equilibria that we decided to consider, namely the binding of NMBA to the acetylcholine (AChR) receptor and to Calabadion 2 as well as the binding of drug to Calabadion 2. With a knowledge of the three K_a values (K_1 – K_3) and the total concentrations of NMBA, AChR and drug it is possible to calculate the concentrations of each species present at equilibrium. It should be noted that the total concentration of displacing drug in this model represent an upper limit to what would be observed *in vivo* because drugs can also be bound to plasma proteins and are subject to rapid distribution to peripheral compartments such as the intercellular space. Accordingly, our model is a conservative screening technique that will generally overestimate the displacement potential of a given drug. Our goal of the simulations was to systematically explore the influence of the different K_a values and total concentrations on the equilibrium concentration of the AChR•NMBA complex since the occupation of the biological receptor by NMBA is ultimately what controls the biological function. The

Table 1. Binding constants determined by direct or competitive UV/Vis assays or direct ^{1}H NMR titrations for the interaction between **2** and drugs **3-29**, drug dosages in the rat model, estimated plasma concentrations, and binding constants toward **1**.

Drug	K_a with **2** (M^{-1})	Dosage in rat model (mg/kg)[28]	Est. Plasma Concentration in Rats (μM)	K_a with **1** (M^{-1})[22]
Acetylcholine chloride	$(1.8 \pm 0.2) \times 10^{5}$ d)	-	-	-
Cisatracurium besylate	$(4.8 \pm 0.9) \times 10^{6}$ d)	0.7	18.3	4.89×10^{3}
Vecuronium bromide	$(1.6 \pm 0.2) \times 10^{9}$ d)	0.7	26.7	5.72×10^{6}
Rocuronium bromide	$(3.4 \pm 0.6) \times 10^{9}$ d)	3.5	160	1.79×10^{7}
3	$(2.0 \pm 0.4) \times 10^{3}$ a)	10	763	2.50×10^{4}
4	$(2.3 \pm 0.2) \times 10^{3}$ b)	10-20	819	$<1.00 \times 10^{3}$
5	$(3.0 \pm 0.4) \times 10^{3}$ a)	10-20	997	$<1.00 \times 10^{3}$
6	$(3.0 \pm 0.6) \times 10^{3}$ a)	10-20	752	$<1.00 \times 10^{3}$
7	$(4.6 \pm 0.5) \times 10^{3}$ a)	10-40	1040	$<1.00 \times 10^{3}$
8	$(5.9 \pm 0.5) \times 10^{3}$ c)	100-300	32122	$<1.00 \times 10^{3}$
9	$(5.9 \pm 1.8) \times 10^{3}$ a)	45-80	4696	$<1.00 \times 10^{3}$
10	$(8.6 \pm 0.8) \times 10^{3}$ c)	0.5-1	63.1	$<1.00 \times 10^{3}$
11	$(1.4 \pm 0.4) \times 10^{4}$ a)	3-100	5948	$<1.00 \times 10^{3}$
12	$(2.1 \pm 0.2) \times 10^{4}$ c)	0.5-2	88.5	-
13	$(3.3 \pm 1.0) \times 10^{4}$ a)	5-10	355	2.40×10^{4}
14	$(4.4 \pm 0.3) \times 10^{4}$ c)	20	335	1.78×10^{4}
15	$(4.8 \pm 0.3) \times 10^{4}$ c)	20-40	1615	1.12×10^{4}
16	$(8.3 \pm 0.6) \times 10^{4}$ c)	0.001	0.12	-
17	$(1.9 \pm 0.1) \times 10^{5}$ c)	6.25-12.5	709	1.02×10^{4}
18	$(1.9 \pm 0.1) \times 10^{5}$ c)	0.018	1.67	$<1.00 \times 10^{3}$
19	$(2.5 \pm 0.1) \times 10^{5}$ c)	0.005-0.015	1.60	$<1.00 \times 10^{3}$
20	$(5.3 \pm 0.4) \times 10^{5}$ c)	0.2-0.4	9.60	2.44×10^{4}
21	$(5.9 \pm 0.7) \times 10^{5}$ c)	-	-	-
22	$(8.0 \pm 0.7) \times 10^{5}$ c)	0.01-0.1	3.04	1.84×10^{4}
23	$(8.2 \pm 0.9) \times 10^{5}$ c)	20	1532	-
24	$(9.3 \pm 0.9) \times 10^{5}$ c)	0.1-0.3	18.2	$<1.00 \times 10^{3}$
25	$(9.7 \pm 1.1) \times 10^{5}$ c)	0.02-0.15	14.0	2.61×10^{4}
26	$(9.8 \pm 0.5) \times 10^{5}$ c)	1-2	133	-
27	$(2.8 \pm 0.1) \times 10^{6}$ c)	0.25-0.45	21.4	$<1.00 \times 10^{3}$
28	$(3.3 \pm 0.5) \times 10^{6}$ c)	0.02-0.05	1.22	$<1.00 \times 10^{3}$
29	$(4.5 \pm 0.7) \times 10^{6}$ c)	6-10	553	5.40×10^{3}

a) measured by direct ^{1}H NMR titration. b) measured by direct UV/Vis titration, c) measured by UV/Vis competition assay using rhodamine 6G, d) reference 17.

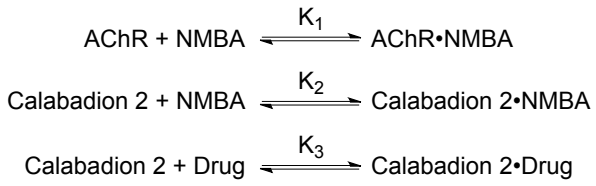

Figure 9. Illustration of the equilibria considered in the simulations using Gepasi.

simulations are meant to inform and serve as a stepping stone toward future *in vivo* selectivity experiments which will ultimately determine the selectivity of **2** towards NMBAs over other drugs in the actual biological system.

Simulation of in vivo equilibria using modelling software Gepasi. We decided to perform the simulations using the freely available software package Gepasi[23] which is capable of performing both kinetic and thermodynamic simulations of user defined interaction networks. The Gepasi software is very powerful and capable of performing multiple simulations where one or more variables are scanned sequentially (using the scan function), which allowed us to develop insight into the influence of each variable. The equilibrium concentrations of each species determined by the Gepasi simulations were exported to and visualized using Microsoft Excel. Below we present simulations using values derived from the data for rocuronium and cisatracurium. An analogous simulation for vecuronium is presented in the Supporting Information.

In vitro selectivity of Calabadion 2 for rocuronium. For the simulations using **2**, rocuronium, and drugs **3** – **29** we fixed the equilibrium constants K_2 (3.4×10^{9} M^{-1}) and K_3 using the values in Table 1. We set the total concentration of rocuronium equal to 160 μM to mimic the initial *in vivo* plasma concentration in the rat; this value was calculated based on the known dosage (3.5 mg/kg, twice the ED90), the average mass (370 g) and the average plasma volume (15.2 mL) of the male Sprague-Dawley rats used in our previous experiments.[29] The initial concentration of AChR was defined as equal to the initial concentration of NMBA (160 μM) for simplicity. Figure 10 shows a three dimensional plot of the mole fraction of

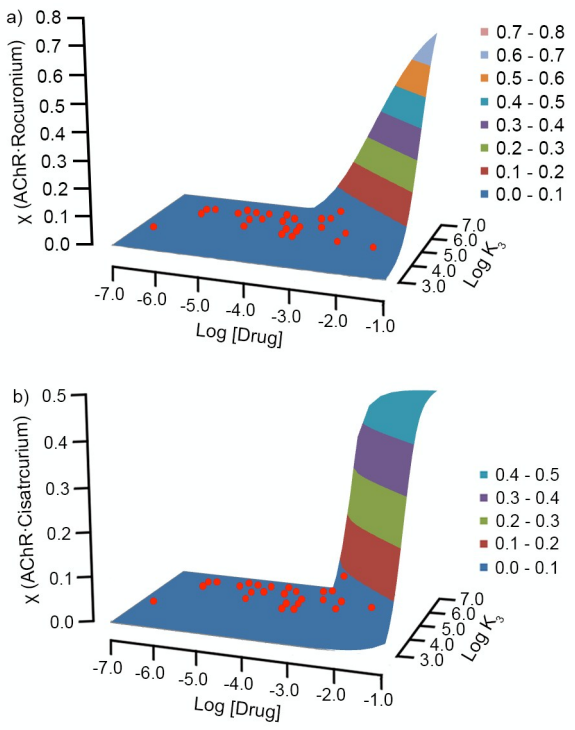

Figure 10. Three dimensional surface plots of the concentration of AChR•NMBA at equilibrium versus log [Drug] and log K_3 for **2**•Drug) for: a) rocuronium at [rocuronium] = [AChR] = 160 μM, [**2**] = 320 μM (2 eqv.), $K_1 = 10^5\ M^{-1}$, $K_2 = 3.4 \times 10^9\ M^{-1}$; b) cisatracurium at [cisatracurium] = [AChR] = 18 μM, [**2**] = 1.2 mM (64 eqv.), $K_1 = 10^5\ M^{-1}$, $K_2 = 4.8 \times 10^6\ M^{-1}$. The red dots mark the points corresponding to each of the 27 drugs (**2** – **29**).

AChR•Rocuronium (z–axis) as a function of the total concentration of drug (e.g. **3** – **29**, x-axis), and log K_3 (y-axis) obtained from the simulations. The range of the x-axis from 0.1 μM to 100 mM was chosen to span the range of plasma concentrations of drug **3** – **29** given in Table 1 whereas the range of the y-axis from 10^3 to $10^7\ M^{-1}$ was chosen to span the range of K_3 values given in Table 1 for drugs **3** – **29**. This surface plot represents the general behavior of $[AChR•Rocuronium]_{equilibrium}$ over the full range of dosages and K_3 of potentially interfering drugs studied in this work. As can be readily seen, there is a plateau region in the lower left region of the plot that corresponds to situations where the drugs do not display any ability to displace rocuronium from the **2**•rocuronium complex and therefore [AChR•rocuronium] is low. Conversely, as [Drug] and/or log K_3 is increased the [AChR•rocuronium] increases. The region in the upper right hand side of the plot corresponds to situations where drugs with these combinations of [Drug] and log K_3 values are expected to display the ability to displace rocuronium from the **2**•rocuronium complex resulting in the increase in the concentration of AChR•rocuronium. The data points corresponding to the individual combinations of plasma concentrations and K_3 values for each drug are marked on the 3D surface of Figure 10a as red dots. According to the constraints of this simulation, none of the drugs possess any substantial ability to displace rocuronium from **2**•rocuronium. From the shape of Figure 10a, it is easy to see that drugs with a combination of a high value of K_3 and a large dose are most likely to displace rocuronium from **2**•rocuronium.

In vitro selectivity of Calabadion 2 for Cisatracurium. The binding affinity of **2** toward the NMBA (K_2) relative to potentially competing drugs plays a major role in influencing how much NMBA is bound to the AChR at equilibrium. Calabadion 2 (**2**) binds cisatracurium ($K_2 = (4.8 \pm 0.9) \times 10^6\ M^{-1}$) approximately 10^3-fold weaker than rocuronium ($K_2 = (3.4 \pm 0.6) \times 10^9\ M^{-1}$) and therefore we would expect that the potential for displacement of cisatracurium from the **2**•cistracurium complex by drugs **3** – **29** would be more significant than for rocuronium. For the purpose of the simulations, we created a three dimensional plot of the equilibrium concentration of AChR•cisatracurium (z-axis) as a function of the concentration of the potentially interfering drug over a range of concentrations (1 μM – 100 mM, full range of average dosage of drugs **3** – **29**, Table 1, x-axis), and the change in K_3 over the range 10^3 – $10^7\ M^{-1}$ (range of K_a values measured for drugs **3** – **29** with **2**, Table 1, y-axis) as shown in Figure 10b. For this simulation, we fixed the total concentration of cisatracurium at 18.3 μM (Table 1) and the concentration of Calabadion 2 at 1183 μM (64 equivalents) which is derived from our previous *in vivo* experiments which found that a dose of 80 mg/kg was effective at reversing cisatracurium. As for the case of rocuronium, we fixed $K_1 = 10^5\ M^{-1}$ and [AChR] as 18.3 μM. Figure 10b represents the general behavior of [AChR•cisatracurium] over the full range of drug concentrations and K_3 values of potentially interfering drugs studied in this work. Similar to the case of rocuronium, there is a large plateau region where [AChR•Rocuronium] is low and displacement of cisatracurium from the **2**•cisatracurium complex is not significant. The upper right side of the Figure 10b is the region where both drug concentration and K_3 are high and where the displacement of cisatracurium from the **2**•cisatracurium complex is most significant. The data points corresponding to the individual concentrations and K_3 values for each drug are marked on the 3D surface of Figure 10b as red dots. Once again, all of the drugs lie in the plateau region which indicates that they do not displace cisatracurium from the **2**•cistracurium complex. Simulations using lower doses of **2** (32 or 16 equivalents) display higher equilibrium mole fractions of AChR•cisatacurium for drugs **29** and **23** (Supporting Information). Of course, the dramatic simplifications introduced into our model means that future *in vivo* experiments are needed to determine if drugs with high combinations of K_3 and dosage (e.g ranitidine (**29**) and imipramine (**23**)) nearby the edge of the plateau result in displacement of **2**•cisatracurium in practice. In this regard, it is worth mentioning that we previously found that the *in vivo* onset and duration of action of succinylcholine (**27**) with its high K_3 value ($2.7 \times 10^6\ M^{-1}$) is unaffected by prior treatment with **2**.[20] Accordingly, the fact that a drug possesses a high K_3 value toward **2** is insufficient to conclude that undesirable displacement interactions will occur.

Influence of K_1. The simulations described above assessed the influence of a range of [Drug] and K_3 values on [AChR•rocuronium] or [AChR•cisatracurium] but were conducted at a single value of K_1 (10^5 M^{-1}) that was not drawn from experimental data, but rather based on the known *in vivo* ability of **2** to function as a reversal agent for rocuronium and cisatracurium. Accordingly, we thought it was important to study the influence of K_1 on the equilibrium concentration of AChR•rocuronium. Figure 11a shows the simulations performed where K_1 is scanned from 10^4 to 10^7 M^{-1} and where [**2**] = 320 μM, [rocuronium] = 160 μM, K_2 = 3.4 x 10^9 M^{-1}, and [drug] and K_3 are taken from Table 1. As can be readily seen, as K_1 is increased the concentration of AChR•rocuronium increases because the difference in free energy between AChR•rocuronium and **2**•rocuronium decreases. At high values of K_1 the concentration of AChR•rocuronium is most significant for ranitidine (**29**). The reason ranitidine possesses the highest potential to displace rocuronium from **2**•rocuronium to form **2•29** is due not only to its relatively high binding constant (K_3 = (4.5 ± 0.7) x 10^6 M^{-1}) but also due to its high therapeutic dose (6-10 mg/kg) which served as inputs to the simulation. Three other drugs that display significant amounts of AChR•rocuronium at high K_1 values are **23**, **17**, and **15** (Figure 11a) which similarly possess a combination of moderate to large K_3 and high therapeutic dose values. Figure 11b shows the simulation of the system when [**2**] is increased to 960 μM (6-fold higher than rocuronium). As can be seen, the concentration of AChR•rocuronium at equilibrium is decreased in all cases relative to Figure 11a. However, the effect is most dramatic for compound **29** which has the highest K_a value but the lowest therapeutic concentrations among **29**, **23**, **17** and **15**. The excess of **2** therefore sequesters more significant amounts of **29** as its **2•29** complex than is possible for **23**, **17**, and **15** with their higher therapeutic concentrations. Overall, this simulation establishes that: 1) the potential for displacement of NMBA from the **2**•NMBA complex is reduced by maximizing the difference between K_2 and K_1, and 2) that the use of concentrations of **2** at the level of the therapeutic concentration of the competing drug can be used to reduce displacement of the **2**•NMBA complex.

Influence of [AChR]. Lastly, in the simulations described above, we have somewhat arbitrarily fixed [AChR] as being equal to the concentration of NMBA. Therefore, we decided to investigate the influence of [AChR] on [AChR•rocuronium] in the presence of ranitidine ([**29**] = 553 μM) by performing simulations with [AChR] spanning the 1.6 μM to 16000 μM range. The other variables were fixed as follows: [rocuronium] = 160 μM, [**2**] = 320 μM, K_1 = 10^5 M^{-1}, K_2 = 3.4 x 10^9 M^{-1}, and K_3 = 4.5 x 10^6 M^{-1}. Figure 12 shows plots of the mole fraction of AChR•rocuronium relative to [AChR] (left axis) and relative to [Rocuronium] (right axis) as a function of [AChR]. These two curves cross when [AChR] = [rocuronium] = 160 μM. At low [AChR] the mole fraction of AChR•rocuronium is ≈ 5%; as [AChR] increases beyond the fixed concentration of rocuronium (160 mM) the mole fraction of AChR•rocuronium drops by necessity. Conversely, if [AChR] is high then the mole fraction of AChR•rocuronium increases because of Le Chateliers principle.

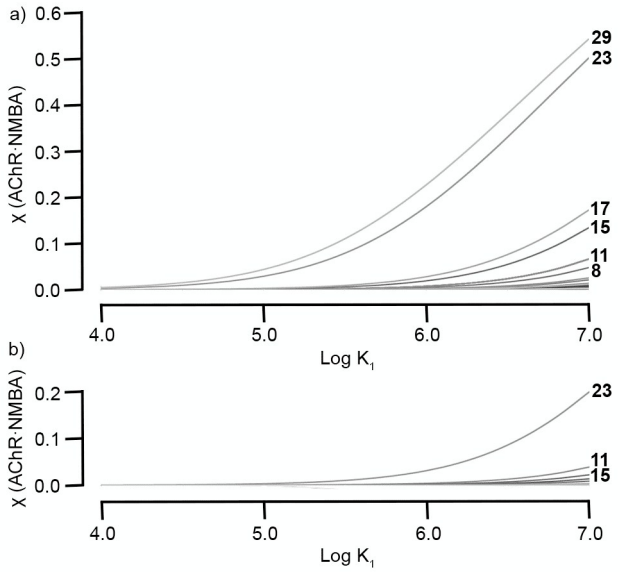

Figure 11. Plot of the mole fraction of AChR•rocuronium versus log (K_1) for drugs **3** – **19** present at their estimated plasma concentrations from Table 1. a) $[\mathbf{2}]_{initial}$ = 320 μM (2-fold higher than $[Rocuronium]_{initial}$), and b) $[\mathbf{2}]_{initial}$ = 960 μM (6-fold higher than $[Rocuronium]_{initial}$).

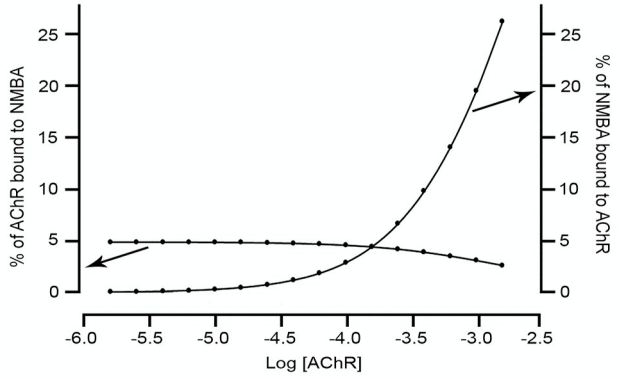

Figure 12. Plot of mole fraction of AChR•rocuronium versus log [AChR].

Conclusions

In summary, we measured the binding constants for the complexes between **2** and drugs **3** – **29** by a combination of direct ^{1}H NMR titrations, direct UV/Vis titrations, and competitive UV/Vis binding assays using the **2**•rhodamine 6G complex. The binding constants range from 2000 M^{-1} (for **3**) to 4.5 x 10^6 M^{-1} (for **29**). The 1:1 stoichiometry of the complexes were confirmed by Job plots whereas the complexation induced changes in ^{1}H NMR chemical shift were used to shed light on the geometry of selected **2**•drug complexes. The x-ray crystal structure of the **2**•ranitidine complex showed: 1) the expected inclusion of the furan ring in the cavity of **2**, 2) the ammonium ion bound at the C=O portal, and 3) an end-to-end helical twist of the acyclic CB[n] receptor **2**. Simulations were performed to

assess the potential for drugs **3** – **29** to displace NMBA from the **2**•NMBA complex resulting in the formation of AChR•NMBA complex. Global simulations reveal that drugs that possess high values of K_3 and/or high therapeutic concentrations have the highest potential to display displacement interactions. For rocuronium and vecuronium none of the drugs display significant displacement potential although ranitidine (**29**) should be assessed in future *in vivo* studies. For cisatracurium, drugs **29** and **23** display both high dose and high K_3 and lie near the edge of the plateau in Figure 10b and consequently must be closely evaluated in future *in vivo* studies. The more significant potential for displacement seen in the cisatracurium simulations can be traced to fact that K_2 for **2**•cisatracurium ($K_2 = (4.8 \pm 0.9) \times 10^6\ M^{-1}$), is 700-fold lower than for **2**•rocuronium ($K_2 = (3.4 \pm 0.6) \times 10^9\ M^{-1}$). In conclusion, we have established that Calabadion **2** displays good to high levels of selectivity toward the NMBAs rocuronium, vecuronium, and cisatracurium both *in vitro* and in simulations designed to capture the essence of the biological system. The studies serve as a guide that allows us to prioritize the investigation of the efficacy of **2** as a reversal agent for neuromuscular block when other drugs (e.g. **3** – **29**) have already been or need to be subsequently administered. The results presented in this work further establish the high potential of Calabadion 2 (**2**) as a broad spectrum reversal agent for both amino-steroidal as well as benzylisoquinolinium type NMBAs.

Acknowledgements

L.I. thanks the Maryland Technology Development Corporation and the National Institutes of Health (CA168365 to L.I.) for financial support. M.E. thanks the Department of Anesthesia, Critical Care, and Pain Medicine financial support. S.G. thanks the University of Maryland for the Gary and Sue Christian Graduate Award.

Conflict of Interest

L.I and M.E. are co-founders of and hold an equity interest in Calabash Bioscience, Inc. which aims to develop Calabadion 2 for biomedical applications.

Notes and references

† Department of Chemistry and Biochemistry, University of Maryland, College Park, Maryland 20742, United States. ‡Department of Anesthesia, Critical Care and Pain Medicine, Massachusetts General Hospital, and Harvard Medical School, Boston, Massachusetts.

*Please address correspondence to Lyle Isaacs (lisaacs@umd.edu) or Matthias Eikermann (meikermann@partners.org).

†Electronic Supplementary Information (ESI) available: Details of 1H NMR and UV/Vis binding measurements and analysis, ^{1}H NMR stack plots, Job plots, Gepasi simulation for vecuronium. Crystallographic information file (.cif) for **2**•**29** (CCDC 1434753). See DOI: 10.1039/b000000x/

1) Raghavendra, T. *J. R. Soc. Med.* **2002**, *95,* 363.
2) Maybauer, D. M.; Geldner, G.; Blobner, M.; Puehringer, F.; Hofmockel, R.; Rex, C.; Wulf, H. F.; Eberhart, L.; Arndt, C.; Eikermann, M. *Anaesthesia* **2007**, *62,* 12; Butterly, A.; Bittner, E. A.; George, E.; Sandberg, W. S.; Eikermann, M.; Schmidt, U. *Br. J. Anaesth.* **2010**, *105,* 304.
3) Adam, J. M.; Bennett, D. J.; Bom, A.; Clark, J. K.; Feilden, H.; Hutchinson, E. J.; Palin, R.; Prosser, A.; Rees, D. C.; Rosair, G. M.; Stevenson, D.; Tarver, G. J.; Zhang, M.-Q. *J. Med. Chem.* **2002**, *45,* 1806; Bom, A.; Bradley, M.; Cameron, K.; Clark, J. K.; Van Egmond, J.; Feilden, H.; MacLean, E. J.; Muir, A. W.; Palin, R.; Rees, D. C.; Zhang, M.-Q. *Angew. Chem., Int. Ed.* **2002**, *41,* 265; Cameron, K. S.; Clark, J. K.; Cooper, A.; Fielding, L.; Palin, R.; Rutherford, S. J.; Zhang, M. Q. *Org. Lett.* **2002**, *4,* 3403.
4) Naguib, M. *Anesth. Analg.* **2007**, *104,* 575.
5) Epemolu, O.; Bom, A.; Hope, F.; Mason, R. *Anesthesiology* **2003**, *99,* 632; Sorgenfrei, I. F.; Norrild, K.; Larsen, P. B.; Stensballe, J.; Ostergaard, D.; Prins, M. E.; Viby-Mogensen, J. *Anesthesiology* **2006**, *104,* 667; Duvaldestin, P.; Kuizenga, K.; Saldien, V.; Claudius, C.; Servin, F.; Klein, J.; Debaene, B.; Heeringa, M. *Anesth. Analg.* **2009**, *110,* 74.
6) Lee, J. W.; Samal, S.; Selvapalam, N.; Kim, H.-J.; Kim, K. *Acc. Chem. Res.* **2003**, *36,* 621.
7) Nau, W. M.; Florea, M.; Assaf, K. I. *Isr. J. Chem.* **2011**, *51,* 559; Masson, E.; Ling, X.; Joseph, R.; Kyeremeh-Mensah, L.; Lu, X. *RSC Adv.* **2012**, *2,* 1213; Isaacs, L. *Acc. Chem. Res.* **2014**, *47,* 2052.
8) Ong, W.; Kaifer, A. E. *Organometallics* **2003**, *22,* 4181.
9) Mock, W. L.; Shih, N.-Y. *J. Org. Chem.* **1986**, *51,* 4440; Liu, S.; Ruspic, C.; Mukhopadhyay, P.; Chakrabarti, S.; Zavalij, P. Y.; Isaacs, L. *J. Am. Chem. Soc.* **2005**, *127,* 15959.
10) Cao, L.; Sekutor, M.; Zavalij, P. Y.; Mlinaric-Majerski, K.; Glaser, R.; Isaacs, L. *Angew. Chem., Int. Ed.* **2014**, *53,* 988.
11) Biedermann, F.; Uzunova, V. D.; Scherman, O. A.; Nau, W. M.; De Simone, A. *J. Am. Chem. Soc.* **2012**, *134,* 15318.
12) Rekharsky, M. V.; Mori, T.; Yang, C.; Ko, Y. H.; Selvapalam, N.; Kim, H.; Sobransingh, D.; Kaifer, A. E.; Liu, S.; Isaacs, L.; Chen, W.; Moghaddam, S.; Gilson, M. K.; Kim, K.; Inoue, Y. *Proc. Natl. Acad. Sci. U. S. A.* **2007**, *104,* 20737.
13) Moghaddam, S.; Yang, C.; Rekharsky, M. V.; Ko, Y. H.; Kim, K.; Inoue, Y.; Gilson, M. K. *J. Am. Chem. Soc.* **2011**, *133,* 3570.
14) Kim, K.; Kim, D.; Lee, J. W.; Ko, Y. H.; Kim, K. *Chem. Commun.* **2004**, 848; Ko, Y. H.; Kim, E.; Hwang, I.; Kim, K. *Chem. Commun.* **2007**, 1305; Angelos, S.; Khashab, N. M.; Yang, Y.-W.; Trabolsi, A.; Khatib, H. A.; Stoddart, J. F.; Zink, J. I. *J. Am. Chem. Soc.* **2009**, *131,* 12912; Biedermann, F.; Rauwald, U.; Cziferszky, M.; Williams, K. A.; Gann, L. D.; Guo, B. Y.; Urbach, A. R.; Bielawski, C. W.; Scherman, O. A. *Chem. - Eur. J.* **2010**, *16,* 13716; Ghosh, S.; Isaacs, L. *J. Am. Chem. Soc.* **2010**, *132,* 4445; Kim, C.; Agasti, S. S.; Zhu, Z. J.; Isaacs, L.; Rotello, V. M. *Nat. Chem.* **2010**, *2,* 962; Kim, E.; Kim, D.; Jung, H.; Lee, J.; Paul, S.; Selvapalam, N.; Yang, Y.; Lim, N.; Park, C. G.; Kim, K. *Angew. Chem., Int. Ed.* **2010**, *49,* 4405; Nguyen, H. D.; Dang, D. T.; van Dongen, J. L. J.; Brunsveld, L. *Angew. Chem., Int. Ed.* **2010**, *49,* 895; Chinai, J. M.; Taylor, A. B.; Ryno, L. M.; Hargreaves, N. D.; Morris, C. A.; Hart, P. J.; Urbach, A. R. *J. Am. Chem. Soc.* **2011**, *133,* 8810; Ghale, G.; Ramalingam, V.; Urbach, A. R.; Nau, W. M. *J. Am. Chem. Soc.* **2011**, *133,* 7528; Walker, S.; Oun, R.; McInnes, F. J.; Wheate, N. J. *Isr. J. Chem.* **2011**, *51,* 616; Ghosh, I.; Nau, W. M. *Adv. Drug Delivery Rev.* **2012**, *64,* 764; Zhang, J.; Coulston, R. J.; Jones, S. T.; Geng, J.; Scherman, O. A.; Abell, C. *Science* **2012**, *335,* 690; Chen, H.; Y-W., C. J.; Li, S.; Liu, J. J.; Wyman, I.; Lee, S. M.-Y.; Macartney, D. H.; Wang, R. *RSC Adv.* **2015**, *5,* 63745; Lee, H. H.; Choi, T. S.; Lee, S. J.; Lee, J. W.; Park, J.; Ho, Y. H.; Kim, W. J.; Kim, K.; Kim, H. I. *Angew. Chem., Int. Ed.* **2014**, *53,* 7461; Li, S.; Chen, H.; Yang, X.; Bardelang, D.; Wyman, I. W.; Wan, J.; Lee, S. M. Y.; Wang, R. *ACS Med. Chem. Lett.* **2015**, DOI: 10.1021/acsmedchemlett.5b00372.
15) Macartney, D. H. *Future Med. Chem.* **2013**, *5,* 2075; Gamal-Eldin, M. A.; Macartney, D. H. *Can. J. Chem.* **2014**, *92,* 243.
16) Ma, D.; Hettiarachchi, G.; Nguyen, D.; Zhang, B.; Wittenberg, J. B.; Zavalij, P. Y.; Briken, V.; Isaacs, L. *Nat. Chem.* **2012**, *4,* 503; Minami, T.; Esipenko, N. A.; Zhang, B.; Isaacs, L.; Nishiyabu, R.; Kubo, Y.; Anzenbacher, P. *J. Am. Chem. Soc.* **2012**, *134,* 20021; Minami, T.; Esipenko, N.; Akdeniz, A.; Zhang, B.; Isaacs, L.; Anzenbacher, P. *J. Am. Chem. Soc.* **2013**, *135,* 15238; Oun, R.; Floriano, R. S.; Isaacs, L.; Rowan, E. G.; Wheate, N. J. *Toxicol. Res.* **2014**, *3,* 447.
17) Ma, D.; Zhang, B.; Hoffmann, U.; Sundrup, M. G.; Eikermann, M.; Isaacs, L. *Angew. Chem., Int. Ed.* **2012**, *51,* 11358.
18) Shen, C.; Ma, D.; Meany, B.; Isaacs, L.; Wang, Y. *J. Am. Chem. Soc.* **2012**, *134,* 7254.
19) Ma, D.; Zavalij, P. Y.; Isaacs, L. *J. Org. Chem.* **2010**, *75,* 4786.

20) Haerter, F.; Simons, J. C.; Foerster, U.; Duarte, I. M.; Diaz-Gil, D.; Ganapati, S.; Eikermann-Haerter, K.; Ayata, C.; Zhang, B.; Blobner, M.; Isaacs, L.; Eikermann, M. *Anesthesiology* **2015**, *123,* DOI: 10.1097/ALN.0000000000000868.
21) Hoffmann, U.; Grosse-Sundrup, M.; Eikermann-Haerter, K.; Zaremba, S.; Ayata, C.; Zhang, B.; Ma, D.; Isaacs, L.; Eikermann, M. *Anesthesiology* **2013**, *119,* 317.
22) Zwiers, A.; van den Heuvel, M.; Smeets, J.; Rutherford, S. *Clin. Drug Invest.* **2011**, *31,* 101.
23) Mendes, P. *Comput. Appl. Biosci.* **1993**, *9,* 563; Mendes, P. *Trends Biochem. Sci.* **1997**, *22,* 361; Mendes, P.; Kell, D. B. *Bioinformatics* **1998**, *14,* 869.
24) Connors, K. A. *Binding constants*; John Wiley & Sons: New York, 1987,
25) Zhang, B.; Isaacs, L. *J. Med. Chem.* **2014**, *57,* 9554.
26) Anslyn, E. V. *J. Org. Chem.* **2007**, *72,* 687.
27) Cao, L.; Isaacs, L. *Supramol. Chem.* **2014**, *26,* 251.
28) Carpenter, W. *Exotic animal formulary*; 4 ed.; Elsevier, 2012; Boston University Research Compliance Rat Formulary. http://www.bu.edu/orccommittees/iacuc/policies-and-guidelines/anesthesia-and-analgesia-in-research-animals/rat-formulary/ (accessed Nov 2015); University of California, San Francisco IACUC Rat Formulary. http://www.iacuc.ucsf.edu/Proc/awRatFrm.asp (accessed Nov 2015).
29) Probst, R. J.; Lim, J. M.; Bird, D. N.; Pole, G. L.; Sato, A. K.; Claybaugh, J. R. *J. Am. Assoc. Lab. Anim. Sci.* **2006**, *45,* 49.